# Force-Force Correlator for Driven Disordered Systems at Finite Temperature

Cathelijne ter Burg and Kay Jörg Wiese
*Laboratoire de Physique de l'Eć ole Normale Supérieure, ENS, Université PSL, CNRS, Sorbonne Université, Université Paris-Diderot, Sorbonne Paris Cité, 24 rue Lhomond, 75005 Paris, France.*

When driving a disordered elastic manifold through quenched disorder, the pinning forces exerted on the center of mass are fluctuating, with mean $f_c = -\overline{F_w}$ and variance $\Delta(w) = \overline{F_w F_0}^c$, where $w$ is the externally imposed control parameter for the preferred position of the center of mass. $\Delta(w)$ was obtained via the functional renormalization group in the limit of vanishing temperature $T \to 0$, and vanishing driving velocity $v \to 0$. There are two fixed points, and deformations thereof, which are well understood: The depinning fixed point ($T \to 0$ before $v \to 0$) rounded at $v > 0$, and the zero-temperature equilibrium fixed point ($v \to 0$ before $T \to 0$) rounded at $T > 0$. Here we consider the whole parameter space of driving velocity $v > 0$ and temperature $T > 0$, and quantify numerically the crossover between these two fixed points.

## I. INTRODUCTION

### A. Generalities

Elastic manifolds driven in a disordered medium have a depinning transition at zero temperature. Typical examples are the motion of domain walls in magnets [1–4], contact line depinning [5], earthquakes [6, 7] and the peeling of a RNA-DNA helix [8]. What these systems have in common is that they are governed by an over-damped equation of motion for the interface $u(x,t)$ which is driven through a quenched disordered medium,

$$\begin{aligned} \partial_t u(x,t) &= \nabla^2 u(x,t) + m^2[w - u(x,t)] \\ &\quad + F\big(x, u(x,t)\big) + \eta(x,t), \\ w &= vt, \qquad v \geq 0. \end{aligned} \tag{1}$$

The disorder forces $F(x,u)$ are short-range correlated, quenched random variables, whereas $\eta(x,t)$ is a thermal noise. Their correlations are

$$\overline{F(x,u)F(x',u')} = \delta(x-x')\Delta_0(u-u'), \tag{2}$$

$$\langle \eta(x,t)\eta(x',t')\rangle = 2T\delta(x-x')\delta(t-t'). \tag{3}$$

The equation of motion (1) can be studied via field theory. Its principle object is the *renormalised force-force correlator* $\Delta(w)$. Interestingly, $\Delta(w)$ is the zero-velocity limit of the connected correlation function of the forces acting on the center of mass $u_w = \frac{1}{L^d}\int_x u(x,t)$ [9]

$$\begin{aligned} \Delta(w) &= \lim_{v\to 0} \Delta_v(w), \\ &= \lim_{v\to 0} L^d m^4 \langle [u_w - w][u_{w'} - w']\rangle^{\mathrm{c}}. \end{aligned} \tag{4}$$

The functional renormalization group (FRG) predicts two distinct universality classes, termed *depinning* and *equilibrium*. Equilibrium is the limit of first $v \to 0$ and then $T \to 0$, whereas depinning is the limit of first $T \to 0$ and then $v \to 0$. In both classes, $\Delta(w)$ has a cusp and admits a scaling form

$$\Delta(w) = m^4 \rho^2 \tilde{\Delta}(w/\rho). \tag{5}$$

Their first distinction is in the scaling of $\rho$,

$$\rho \sim m^{-\zeta}, \tag{6}$$

defining a roughness exponent $\zeta$. The second distinction is the shape function $\tilde{\Delta}(w)$.

The function $\Delta(w)$ was measured in numerical simulations [10, 11], and experiments [2, 4, 5, 12]. These measurements, both in simulations and experiments, are done by moving the center of the confining potential of strength $m^2$ at a small driving velocity $v$. For *depinning*, such measurements were done in soft ferro magnets, both with SR and LR elasticity [4] and DNA/RNA unzipping [8]. In all cases, the measured force-force correlator $\Delta(w)$ agreed with the predictions from field theory, and was rounded by a finite driving velocity $v > 0$. While the experiments above are for zero-temperature depinning, in general the driving velocity $v > 0$ is not the only perturbation and the system is subject to thermal noise at temperature $T > 0$ as in Eq. (1). This prompted us to study the crossover between the two fixed points. Apart from the two fixed points depinning and equilibrium, only small deformations of these fixed points are well understood: For depinning, driving at a finite velocity can be accounted for by folding the zero-velocity fixed point with the response function, which leads to a rounding of the cuspy fixed point [13]. On the other hand, the equilibrium fixed point is rounded by a finite temperature, describable by a boundary layer [14]. The goal of this paper is to describe the crossover between these two limiting cases. We do this by means of numerical simulations. Choosing to work at fixed $m^2$, this is parametrised by $v$ and $T$.

### B. Mean-field description

Since these questions are difficult to treat numerically for an interface, our study is done for a single degree of freedom which can itself be interpreted as the center-of-mass of the interface, or the *mean field*. Denoting the center of mass of the interface by $u(t)$, the equation of motion (1) and noise correlations (2)-(3) reduce to

$$\partial_t u(t) = m^2[w - u(t)] + F(u) + \eta(t), \tag{7}$$

$$\langle \eta(t)\eta(t')\rangle = 2T\delta(t-t'), \tag{8}$$

$$\overline{F(u)F(u')} = \Delta_0(u-u'). \tag{9}$$

The first term is the force exerted by a confining well, i.e. a Hookean spring with spring constant $m^2$. $F(u)$ is the

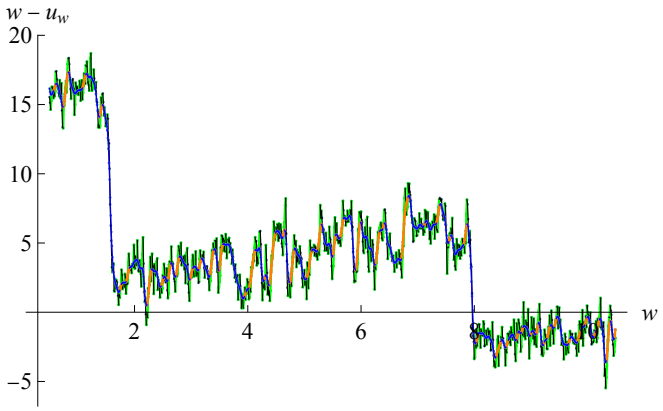


FIG. 1. $w - u_w$ for $\delta t = 10^{-3}$, $v = 0.01$, $m^2 = 0.1$, $T = 0.5$. (DNS). Forward going sections are orange, and backward going sections are blue. Obtained after smoothening of the data in green.

random pinning force, possibly the derivative of a potential $F(u) = -\partial_u V(u)$. Specifying the correlations of $F(u)$ defines the system. Following [13] we consider forces $F(u)$ that describe an Ornstein-Uhlenbeck (OU) process driven by a Gaussian white noise $\xi(u)$

$$\begin{aligned} \partial_u F(u) &= -F(u) + \xi(u), \\ \langle \xi(u)\xi(u')\rangle &= 2\delta(u-u'). \end{aligned} \tag{10}$$

At small distances $u \ll 1$, the forces $F(u)$ have the statistics of a random walk, thus its microscopic limit is the ABBM model [15, 16]. At large distances $w \gg 1$ forces are uncorrelated; this is termed random-field (RF) disorder.

Returning to the equation of motion (7), at zero temperature and at slow driving, most of the time the lhs vanishes. This condition defines the force $F_w$, given $w$, and the associated critical force $f_c$ as

$$F_w = m^2(u_w - w), \tag{11}$$

$$f_c := \lim_{v\to 0} -\overline{F_w} = \lim_{v\to 0} \overline{m^2(w-u_w)}. \tag{12}$$

The signs are such that exerting a positive force $f_c$ overcomes the pinning forces $F(u_w)$. Due to the thermal noise, $u_w$ is a fluctuating variable allowing for motion to occur even below the threshold force by thermal activation over energy barriers $U$. For sufficiently small velocities, this allows the dynamics to equilibrate with activation times following an Arrhenius law $\tau \sim e^{U/T}$. Thermal fluctuations allow for $u_w$ to go backward, violating Middleton[17]. In Fig. 1 this is illustrated with forward segments in orange and backward segments in blue. In green in the background is thermal noise. The effective disorder is defined as

$$\Delta_{v,T}(w) = \overline{F_w F_{w'}}^{\rm c}. \tag{13}$$

We have written a subscripts $v, T$ to remind that measurements depend on both $v$ and $T$. Finally, the critical force is related to the area of the hysteresis loop as

$$m^2[\overline{(w-u_w)}^{\rm forward} - \overline{(w-u_w)}^{\rm backward}] = 2f_c. \tag{14}$$

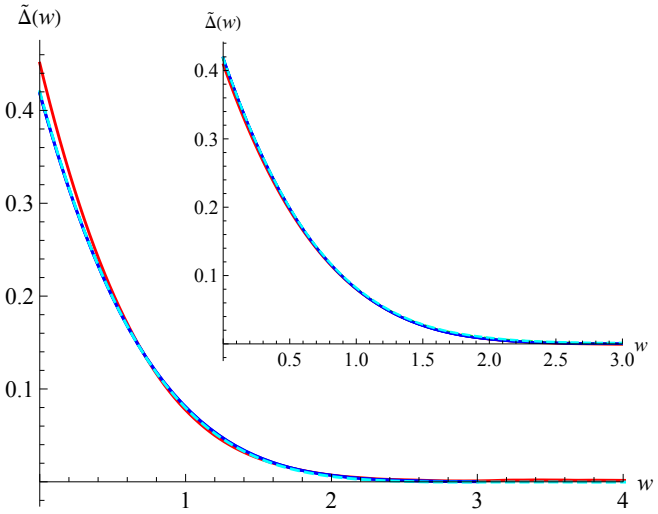


FIG. 2. $\tilde\Delta(w)$ for the Sinai model (blue) obtained by numerical integration of Eqs. (16)-(18). It is compared to the energy minimisation for $m^2 = 0.1$ (red), $m^2 = 0.01$ (cyan dashed) indistinguishable from the theory. Statistical errors are within line thickness. Inset: Idem for the OU model in Eq. (10).

Hysteresis is absent in equilibrium where $f = 0$ and maximal at depinning.

### C. Review of known results for a single perturbation

Before we present our findings answering the questions posed in the introduction, let us review what is known for the single perturbation cases.

#### 1. *Equilibrium fixed point*

The zero-temperature equilibrium fixed point can be measured by energy minimisation (EM) at fixed $w$ of

$$\mathcal{H}_w(u) = \frac{m^2}{2}(u-w)^2 + V(u), \tag{15}$$

see appendix A for implementation details. Here $V(u) = -\int F(u)du$ is the random potential. For the random-field disorder relevant for Eq. (10), the model is known as the Sinai model, first introduced in [18]. The effective force-force correlator reads (see [19], with corrections in [20])

$$\Delta(w) = m^4 \rho_m^2 \tilde\Delta(w/\rho_m), \tag{16}$$

$$\rho_m = 2^{\frac{2}{3}} m^{-\frac{4}{3}} \sigma^{\frac{1}{3}}, \tag{17}$$

$$\tilde{\Delta}(w) = -\frac{\mathrm{e}^{-\frac{w^3}{12}}}{4\pi^{\frac{3}{2}}\sqrt{w}} \int_{-\infty}^{\infty} \mathrm{d}\lambda_1 \int_{-\infty}^{\infty} \mathrm{d}\lambda_2\, \mathrm{e}^{-\frac{(\lambda_1-\lambda_2)^2}{4w}} \times \mathrm{e}^{i\frac{w}{2}(\lambda_1+\lambda_2)} \frac{\mathrm{Ai}'(i\lambda_1)}{\mathrm{Ai}(i\lambda_1)^2} \frac{\mathrm{Ai}'(i\lambda_2)}{\mathrm{Ai}(i\lambda_2)^2} \times \left[1+2w\frac{\int_0^\infty \mathrm{d}V \mathrm{e}^{wV}\mathrm{Ai}(i\lambda_1+V)\mathrm{Ai}(i\lambda_2+V)}{\mathrm{Ai}(i\lambda_1)\mathrm{Ai}(i\lambda_2)}\right]. \tag{18}$$

The roughness exponent is thus $\zeta = 4/3$. Fig. 2 shows in blue the analytical solution of Eqs. (16)-(18). In red and cyan are numerical simulations of Eq. (15) for $\sigma\delta(u-u')$ correlated forces, i.e. $\langle V(u) - V(u')\rangle \sim \sigma|u-u'|$. Already for $m^2 = 0.01$, the simulation has converged to the theory. The inset shows comparison to the model (10) of OU forces, which belongs to the same universality class. Since the microscopic disorder integrates to 1, $\sigma = 1$. At finite temperature, thermal fluctuations smoothen the shocks and round the cusp in a boundary layer $u \sim T$. This is shown in Fig. 3. The size of this boundary layer can be estimated from the FRG [20],

$$\Delta_T^{\mathrm{eq}}(w) = \mathcal{A}_T \Delta^{\mathrm{eq}}(\tilde{w}), \tag{19}$$

$$\tilde{w} = \sqrt{w^2+t^2}, \qquad \frac{t}{\rho} = \frac{3}{\varepsilon}\frac{2Tm^2}{\Delta(0)}, \tag{20}$$

$$\mathcal{A}_T = \frac{\int_0^\infty \mathrm{d}w \Delta^{\mathrm{eq}}(w)}{\int_0^\infty \mathrm{d}w \Delta^{\mathrm{eq}}(\tilde{w})}. \tag{21}$$

The amplitude $\mathcal{A}_T$ ensures normalisation and the area is preserved under thermal rounding. A brief derivation[20] of this set of equations in given in appendix B. The dimensionless temperature $T_m \sim Tm^\theta$ scales with its own exponent, where $\theta = d - 2 + 2\zeta$ is the *equilibrium energy exponent*.

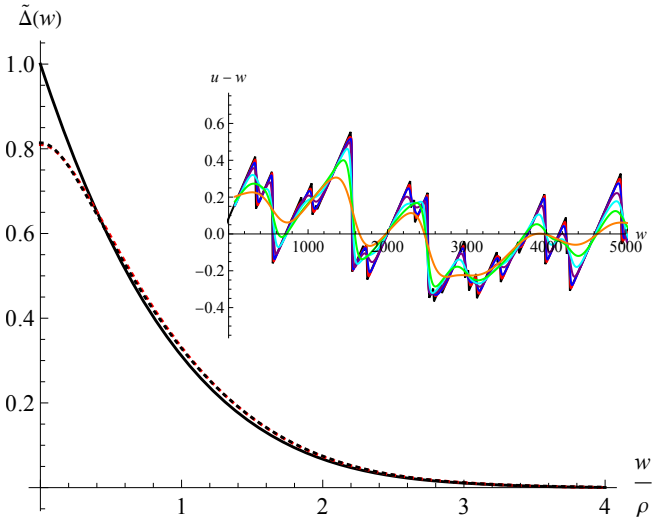


FIG. 3. Boundary layer analysis for equilibrium random field disorder (EM) for the dimensionless rescaled disorder $\tilde{\Delta}(w)$ and rescaled to have unit amplitude and slope 1 at $w = 0$. Black solid, $v = 0, T = 0$ fixed point, black dashed, numerical measurement at $m^2 = 0.01$, $T = 2$, red dotted, thermal boundary layer ansatz using equations (19). Inset: The effective force at various $T$.

A more delicate question is what the dynamical exponent $z$ in equilibrium is. The observation that $z = 2$ in both the free theory as well as at depinning suggests that this likely holds also in equilibrium. Finally, the pinning force $f_c = 0$ in equilibrium.

*Depinning fixed point*

For depinning the effective disorder (4) is given by [21]

$$\Delta(w) = m^4\rho_m^2\tilde{\Delta}_{\mathrm{Gumbel}}(w/\rho_m), \tag{22}$$

$$\tilde{\Delta}_{\mathrm{Gumbel}}(w) = \frac{w^2}{2} + \mathrm{Li}_2(1-e^{|w|}) + \frac{\pi^2}{6}, \tag{23}$$

$$\rho_m = \frac{1}{2m^2\ln(m^{-2})}. \tag{24}$$

The roughness exponent thus is $\zeta = 2^-$; the dynamical exponent is $z = 2^-$ [13]. In the simulations, we can measure (22) at zero velocity, by moving the parabola from $w \to w + \delta w$ and waiting for the dynamics to cede. In an experiment, performed at finite $v$, $\Delta(w)$ is rounded by the driving velocity [13]

$$\Delta_v(w-w') = \iint R(t)R(t')\Delta(w-w'-v(t-t')). \tag{25}$$

By construction, $\int_t R(t) = 1$ and the integral under the depinning fixed point is preserved under velocity perturbations. At small $v$, (25) can be approximated by

$$\Delta_v(w) = \frac{1}{\mathcal{N}}\Delta(\sqrt{w^2+(v\tau)^2}), \tag{26}$$

where $\mathcal{N}$ is chosen s.t. $\int_w \Delta_v(w) = \int_w \Delta(w)$.

At $v = 0$ the critical force $f_c$ defined in (12) is maximal; it decreases at $v > 0$ [13]

$$f_c := \overline{m^2(w-u_w)} - v \tag{27}$$

## II. RESULTS

We now present our numerical results, mostly obtained by direct numerical simulation (DNS). First in section II A we check Eqs. (16)-(21) for equilibrium. In section II B we discuss several order parameters characterizing the crossover between equilibrium and depinning. Section II C shows that with the rescalings established so far, we can collapse all our data.

### A. Equilibrium regime and thermal peak

In Fig. 5 we show the results of numerical simulations of $\Delta_{v,T}(w)$ in the near-equilibrium regime. The presence of the thermal noise leads to a thermal peak (TP) at small $w$. In

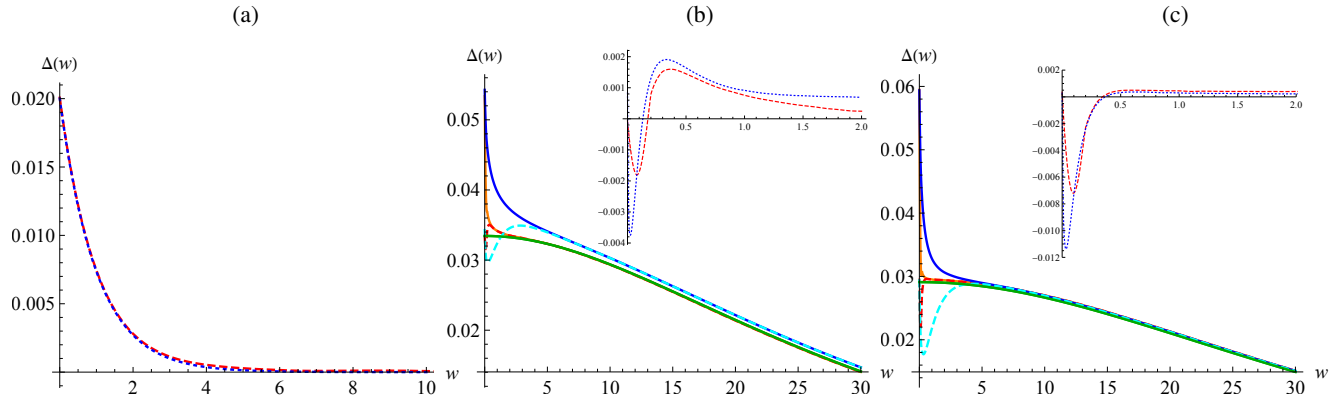


FIG. 4. (a) Comparison of the prediction (28) (blue) for $m^2 = 0.01$, $v = 10^{-3}$, $T = 2$ to a measurement of the noise correlations in the absence of disorder. (b) and (c) are in presence of quenched disorder.
Subfigures (b) and (c): For $m^2 = 0.01$, $T = 2$ (b) and $T = 3$ (c) comparison of the equilibrium $\Delta_T^{\rm eq}(w)$ (green, EM) to $\Delta_{v,T}(w)$ at $v = 10^{-3}$ (blue solid, DNS) and $v = 10^{-4}$ (orange solid, DNS). In dashed cyan/red, we show the combination (30). This correctly captures the amplitude, but a signal of anti-correlations remains. In the inset we show the difference $\delta\Delta_{v,T}(w/v)$, which quantifies the corrections due to non-equilibration.

absence of disorder, it reads

$$\begin{aligned}\Delta_v^{\rm TP}(w-w') &= 2Tm^4\int_{-\infty}^{\infty} R(t,\tau)R(t',\tau)\,{\rm d}\tau \\ &= Tm^2 e^{-m^2|t-t'|} \\ &= Tm^2 e^{-m^2|w-w'|/v}. \end{aligned} \tag{28}$$

Here $R(t) = \Theta(t)e^{-m^2 t}$ is the response function of the free theory. This is checked in Fig. 4(a).

Let us now turn back to the disordered case, at finite velocity $v > 0$ and finite temperature $T > 0$. We make the ansatz

$$\Delta_{v,T}(w) = \Delta_T^{\rm eq}(w) + \Delta_v^{\rm TP}(w) + \delta\Delta_{v,T}(w). \tag{29}$$

The first term is the relevant result for $v = 0$. The second term is the contribution (28) from the thermal noise. If the driving velocity is small enough for the dynamics to equilibrate, then we expect the third term $\delta\Delta_{v,T}(t)$ to vanish, or at least to be small.

Figs. 4(b)-(c) show the combination

$$\Delta_{v,T}(w) - \Delta_v^{\rm TP}(w) = \Delta_T^{\rm eq}(w) + \delta\Delta_{v,T}(w), \tag{30}$$

for $T = 2$ (b) and $T = 3$ (c). Whereas it correctly subtracts the thermal noise at $w = 0$, the remaining term $\delta\Delta_{v,T}(t)$ is visible. In the inset, we show $\delta\Delta_{v,T}(t)$, i.e. the error we make in the approximation $\Delta_{v,T}(w) \approx \Delta_T^{\rm eq}(w) + \Delta_v^{\rm TP}(w)$. We see that despite a difference of $v$ by a factor of ten, the rescaled combination $\delta\Delta_{v,T}(t = w/v)$ at small $t$ depends little on $v$. This estimates the boundary layer in our example to be $\delta t \approx 2$.

Eq. (29) approximately predicts the amplitude for equilibrium,

$$\Delta_{v,T}(0) \approx \Delta_T(0) + m^2 T. \tag{31}$$

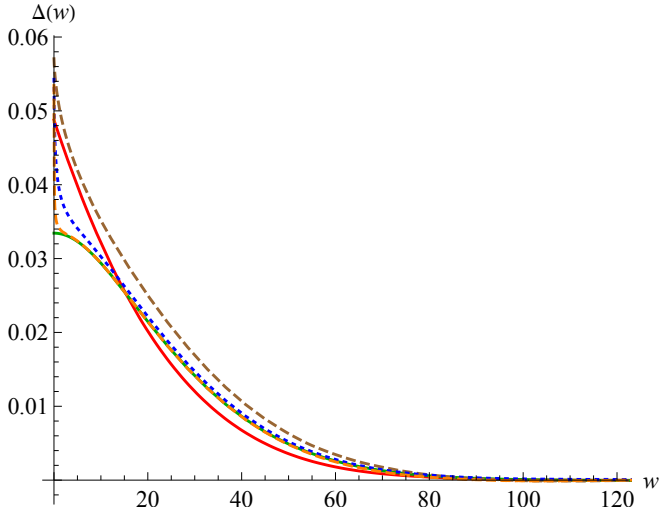


FIG. 5. The equilibrium regime for $T = 2$ with the zero temperature fixed point in red and $\Delta_T(w)$ (EM) shown in green. Simulation of (7) shows $v = 0.01$ (brown), $v = 10^{-3}$ (blue) and $10^{-4}$ (orange) we show $\Delta_{v,T}(w)$ (DNS). For the smallest two driving velocities the agreement is excellent, and the thermal peak, rounded by the driving velocity, is clearly visible. The largest velocity no longer obeys the decomposition (31) and belongs to the crossover regime.

As can be seen in Fig. 5, this relation breaks down for $v = 0.01$, corresponding to $\hat{T} = Tm^{2/3}\ln(v) \approx 2$. A look at Fig. 6, discussed next, shows that there $f/f_{\rm c} \approx 0.05$, which signals the approach to the crossover regime.

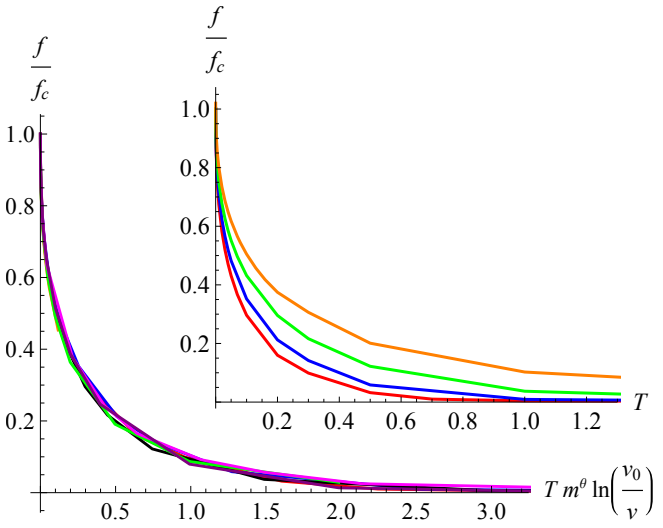


FIG. 6. Scaling collapse of the measured force for $T > 0$, and different $m$, $v$. We found an optimal collapse for $v_0 = 1$, but any $v_0$ of the same order of magnitude does well.

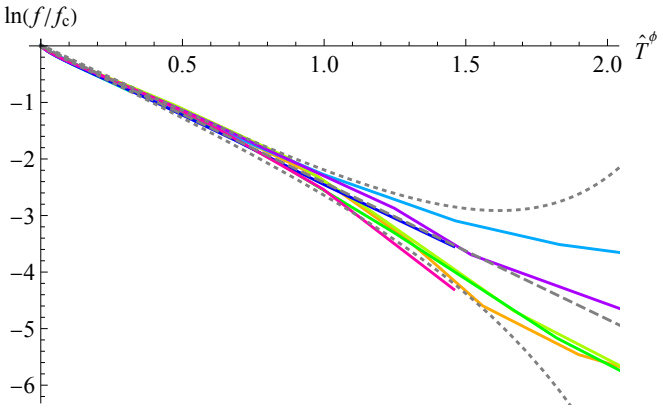


FIG. 7. This plot shows that $f/f_c$ from Fig. 6 is a stretched exponential, with an exponent of about 0.55. Gray dashed is a fit to a linear function, gray dotted putative error bars.

### B. Order parameters

#### 1. *The mean force as an order parameter*

Since the measured pinning force $f$ is maximal at zero-temperature depinning, and vanishes at equilibrium, it is a natural candidate for an order parameter. We define

$$\Psi_f := \frac{f}{f_c}, \tag{32}$$

which vanishes in equilibrium and is 1 at depinning. The inset of Fig. 6 shows this force ratio for different $m^2, T$ and $v$, for $v = 10^{-2}, 10^{-3}, 10^{-4}$, $m^2 = 0.1 - 10^{-3}$ and $T = 0 - 2$. Using that the dimensionless temperature is $Tm^\theta$ and velocity and temperature are related by Arrhenius' law as

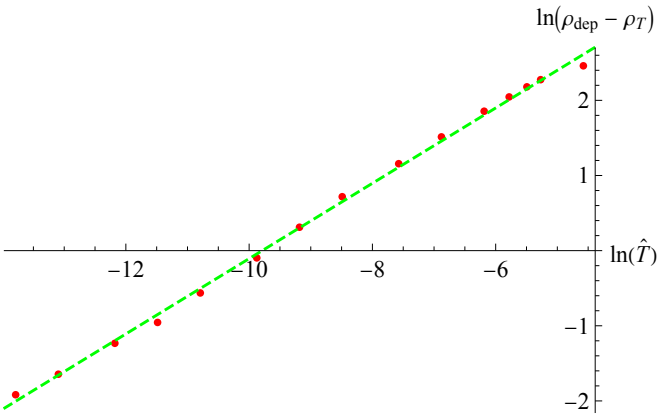


FIG. 8. Check of the scaling relation (35). The green dashed line has a slope of $\phi = 0.50$.

$\ln(v) \sim 1/T$, a natural ansatz for a scaling parameter is

$$\hat{T} := Tm^{2/3} \ln(1/v). \tag{33}$$

This collapses all curves on a single master curve as shown in the main plot of Fig. 6.

We can go one step further. To do so, let us plot the log of $f/f_c$ as a function of $\hat{T}^\phi$. We find on Fig. 7 an almost linear behaviour for an exponent $\phi = 0.55$, with slope $-2.41$. Thus

$$\frac{f}{f_c} \approx \mathrm{e}^{-\left(\frac{\hat{T}}{\hat{T}_c}\right)^\phi}, \qquad \phi \approx 0.55, \quad \hat{T}_c \approx 0.2. \tag{34}$$

is a stretched exponential. Note that if the fit is attempted close to $f \approx f_c$, one can also conclude on $\phi \approx 0.51$. If we restrict to 10 percent deviation, this allows for $\phi$ in a range $\phi \in [0.51, 0.56]$

We expect the regime $f/f_c \to 1$ to be governed by the depinning fixed point, and $f/f_c \to 0$ by the equilibrium fixed point. The crossover regime should be best visible for $f/f_c \approx 1/2$ .

#### 2. *The correlation length as an order parameter*

In section II B 1 we established the mean force as an order parameter between equilibrium and depinning. While this is the most robust quantity, there are other quantities one might use, and compare to their values for zero-temperature depinning. The first is the correlation length $\rho$, which decreases with temperature compared to its value at depinning. If one considers zero-temperature depinning as reference point, then at small temperatures,

$$\rho_{\rm dep} - \rho_T \sim \hat{T}^\phi, \tag{35}$$

with $\phi = 0.50 \pm 0.02$, see Fig. 8.

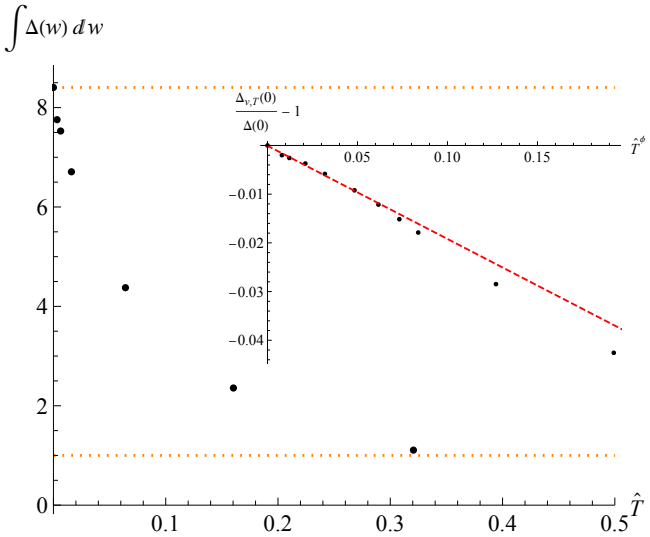


FIG. 9. The change with temperature of the area (main plot) and amplitude at $w = 0$ (inset) for $\phi = 0.56$

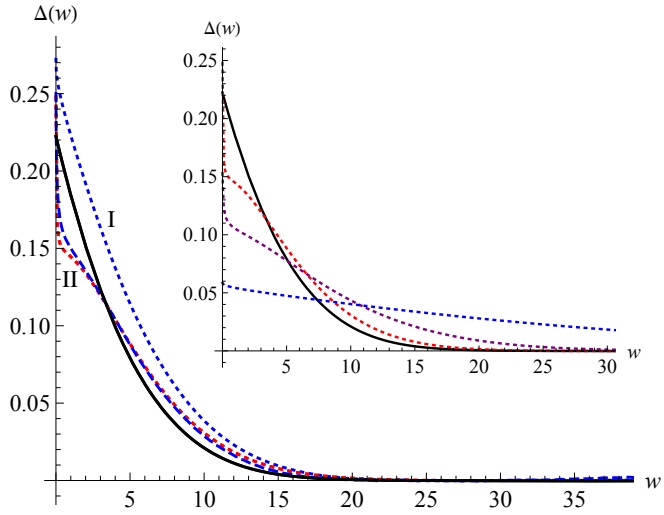


FIG. 10. Scaling of $\Delta(w)$ (DNS). The inset shows the equilibrium fixed point (EM) at $m^2 = 0.1$ (black) and $\Delta_{v,T}(w)$ for $m^2 = 0.1$ (red), $m^2 = 0.05$ (purple) and $m^2 = 0.01$ (blue) for $T = 1, v = 10^{-3}$. Main plot shows the collapse of $m^2 = 0.01$ onto $m^2 = 0.1$ by I) rescaling only $m^2$, II) rescaling in addition $Tm^{\theta}$.

#### 3. *The disorder amplitude as an order parameter*

Assuming that

$$\Delta_{v,T}(w) = m^4 \rho_T^2 \tilde{\Delta}(w/\rho_T), \tag{36}$$

the amplitude $\Delta_{v,T}(0)$ at small $T$ should behave as

$$\frac{\Delta_{v,T}(0)}{\Delta_{\rm dep}(0)} - 1 \simeq \left(\frac{\rho_T}{\rho_{\rm dep}}\right)^2 - 1 \sim T^{\phi} + \mathcal{O}(T^{2\phi}). \tag{37}$$

Our measurements presented in the inset of Fig. 9 are consistent with an exponent in a range $\phi \in [0.5, 0.6]$.

#### 4. *The disorder integral as an order parameter*

Both the correlation length as well as the amplitude are very sensitive to details of the rounding around the cusp. More robust is to consider the area under $\Delta(w)$. The above relations above would imply that

$$\frac{\int_w \Delta_{v,T}(w)}{\int_w \Delta_{\rm dep}(w)} \sim \left(\frac{\rho_T}{\rho_{\rm dep}}\right)^3 \sim T^{\phi} + \mathcal{O}(T^{2\phi}) \tag{38}$$

Our data are consistent with an exponent in the range of $\phi = 0.5$ to $\phi = 0.67$, favoring the upper end. The decrease of the area is shown in Fig. 9. The orange dashed lines are references for depinning (top) and equilibrium (bottom).

### C. Scaling collapses

Let us next consider scaling close to equilibrium and depinning.

#### 1. *Scaling near equilibrium*

For equilibrium

$$\Delta(w) \sim m^{4/3} \tilde{\Delta}(w m^{4/3}). \tag{39}$$

While this scaling holds for all $w$ at the zero-temperature fixed point, the scaling within the boundary layer is more subtle. Consider first the inset of Fig. 10. In black is shown the equilibrium fixed point for $m^2 = 0.1$ and red/blue/purple show from top to bottom $m^2 = 0.1, 0.05, 0.01$ for $T = 1$, $v = 10^{-3}$. In the main plot we perform a scaling collapse from $m^2 = 0.01$ onto $m^2 = 0.1$. In blue dotted (I), we rescaled by only accounting for the difference in mass, i.e. with $m^{4/3}$. One sees it clearly deviates. To obtain a full scaling collapse, one needs to scale also temperature with its corresponding dimension, i.e. $Tm^{-\theta}$ with $\theta = 2/3$, leading to the blue-dashed curve (II). The remaining offset, comes from the velocity which also scales with $m^2$. Using that $z = 2$ both in the free theory and depinning, suggest a scaling of $v \sim m^{2/3}$. A look at the size of the boundary layer of the thermal peak, suggests that the driving velocity should be reduced by a factor 2, which is approximately consistent with the above scaling.

#### 2. *Scaling near depinning*

In Figs. 11 and 12 we show the whole crossover regime from depinning to equilibrium. The previous section studied the change in correlation length and area as an order parameter, but there is more we can say close to depinning. For this consider Fig. 11, at $v = 0.001$. In the inset we use the scaling relation (36) to collapse the curve for $T = 0.02$ onto $T = 0$. In particular, this implies that the shape $\tilde{\Delta}(w)$ is not affected

by temperature. When comparing experimental data to the fixed point theory candidates, this is important as scales are fixed using the correlation length. At larger $T$ this no longer holds true, and the shape changes. Another interesting feature can be identified at a larger driving velocity. Consider Fig. 12 for $v = 0.1$, where the rounding due to the driving velocity is clearly present. As we now know that when approaching equilibrium a thermal peak forms, one would expect some interplay between the velocity boundary layer and the thermal peak. Fig. 12 shows that this is indeed the case. For large $T > 3$ an apparent cusp seems to re-emerge. Its nature however, is very different then the cusps of the depinning and equilibrium fixed points. There is was related to the existence of shocks and avalanches. Here, it is an artefact of the combined effect of the velocity boundary layer and the thermal peak forming on top. This regime corresponds to $\hat{T} = 0.32$ far in the crossover regime of Fig. 6.

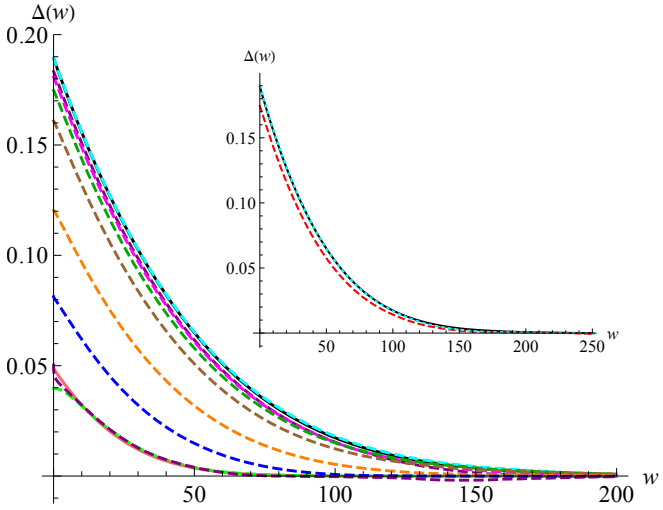


FIG. 11. $\Delta_{v,T}(w)$ (DNS) for $m^2 = 0.01$, $v = 10^{-3}$ and $T \in [0, 0.005, 0.01, 0.02, 0.05, 0.2, 0.5, 1]$ from equilibrium (red, bottom, EM) to depinning (black, top). The inset shows scaling collapse using the scaling relation in (36) for $T = 0.02$. $Tm^\theta \ln 1/v = 0.03$ indeed close to depinning. Brown curve corresponds to $Tm^\theta \ln 1/v = 0.075$ already at 60 % of the maximal value of $f_c$. No scaling collapse could be obtained here.

## III. SUMMARY AND DISCUSSION

In this work we addressed the long-standing question of the full crossover between depinning and equilibrium. Studying the force and the effective force-force correlator for a one-particle model, we characterized the whole phase diagram of finite velocity $v$ and finite temperature $T$. This serves as a reference point to experiments and simulations. We showed that the mean force, divided by the mean force at depinning, is a robust order parameter, allowing one to quantify where in between depinning and equilibrium one is, and what signal one should expect for the force-force correlations.

Our results are directly applicable to the unzipping of a DNA hairpin, and are currently confronted to experiments.

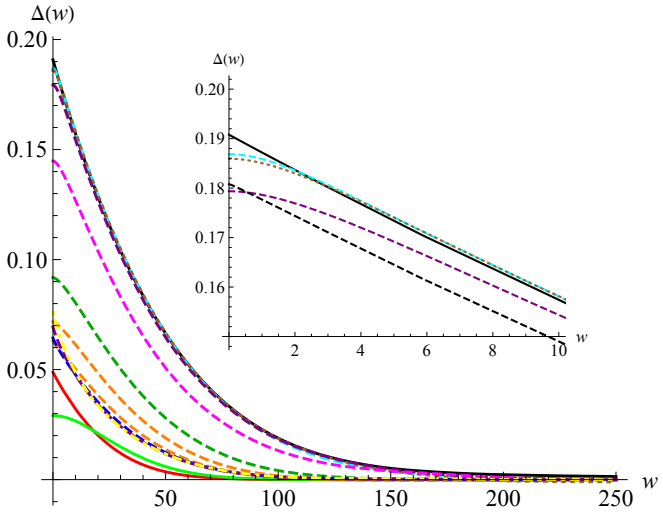


FIG. 12. $\Delta_{v,T}(w)$ (DNS) for $m^2 = 0.01$ at fixed $v = 0.1$ and varying $T$ compared to the depinning (black, top) and equilibrium (red, bottom, EM) and thermal rounding at $T = 5$. From top to bottom temperature increases $T \in [0, 0.001, 0.01, 0.1, 0.5, 1, 2, 3, 4, 5]$. At $T = 3$, the velocity boundary layer disappears due the formation of the thermal peak. Inset shows the small temperature effect on the boundary layer. It is little affected at small $T = 0.001$. Inset black dashed shows $T = 0.01, v = 10^{-3}$ and purple dashed $T = 0.01, v = 10^{-3}$ showing they are not related by velocity unfolding.

This experiment has all the ingredients studied here: It has a finite temperature, it has random forces, and it has a confining potential whose minimum is slowly increasing at a driving velocity $v$, allowing us to measure its force-force correlations. Earlier analysis, [22] has suggested this experiment to be close to equilibrium. Interesting in this experiment is that the stiffness of the trap, ($m^2$ in our notation) decreases during the experiment

$$\frac{1}{m^2} = \frac{1}{m_0^2} + an = \frac{1}{m_0^2} + a'w, \tag{40}$$

where $n$ is the number of unzipped bases, itself proportional to the position of the confining potential $w$, starting with $w = 0$ for the completely closed molecule. Reminding that $m$ sets the renormalization scale, we see that the experiment runs the renormalization group for us! We report more on this experiment in a future publication with P. Rissone, M. Rico-Pasto and F. Ritort.

We hope that this work can serve as a reference work in any situation where both the driving velocity $v$ and temperature $T$ are non-vanishing, and it is a priori not clear where in the phase diagram one is sitting. Looking at the critical force as a ratio its value at depinning, allows one to locate where in the phase diagram one is sitting. One can then asses and quantify all the features discussed here: Thermal rounding, the thermal peak and its broadening as a function of $m^2$, the scaling in the $w$ direction.

## ACKNOWLEDGMENTS

We thank A. Kolton and A. Rosso for sharing their experience, and P. Rissone, M. Rico-Pasto and F. Ritort for the experimental collaboration for DNA unzipping, which has been a source of information for the present work.


### Appendix A: Numerical implementations

The number of samples is denoted

$$N := \text{number of samples.} \tag{A1}$$

In this work we used two numerical implementations:

(i) *Direct numerical simulation (DNS)*. To solve the coupled set of differential equations (7)-(10) we use a space discretization $\delta u = 10^{-2}$ to first obtain the random forces $F(u)$ for $u = n\delta u$, $n \in \mathbb{N}$. $F(u)$ is then linearly interpolated between these points. We finally solve Eq. (7) with the Euler method, using a time-discretization of $\delta t = 10^{-3}$.

(ii) *Exact minimisation (EM)*. In the statics the relevant quantities are computed using minimisation of the energy in Eq. (15). For a given disorder realisation $V(u)$, the minimum of the potential as a function of $w$ is

$$\hat{V}(w) = \min_u \left[ V(u) + \frac{m^2}{2}(u-w)^2 \right], \tag{A2}$$

At finite temperature, this is replaced by

$$\hat{V}(w) = V(w) - T \ln \left( \langle e^{-\frac{V(u)-V(w)}{T} - \frac{m^2}{2T}(u-w)^2} \rangle_u \right). \tag{A3}$$

Using potential differences allows to better restrict the necessary range in $u-w$. For RF disorder, as is the case for the model of OU forces, the potential is obtained by integrating the random forces,

$$V(u) - V(w) = -\int_w^u F(u')\mathrm{d}u'. \tag{A4}$$

The effective force $\hat{F}(w) = -\partial_w \hat{V}$ then becomes

$$\hat{F}(w) = m^2 \frac{\langle e^{-\frac{V(u)-V(w)}{T} - \frac{m^2}{2T}(u-w)^2} (u-w) \rangle_u}{\langle e^{-\frac{V(u)-V(w)}{T} - \frac{m^2}{2T}(u-w)^2} \rangle_u}. \tag{A5}$$

### Appendix B: An auxiliary calculation

The size of the boundary layer can be estimated from the finite $T$ FRG equation for $\tilde{\Delta}(w)$. The computation has been done in [20]. Here we give the relevant results. We define

$$\tilde{\Delta}(w) = \frac{\varepsilon}{3}\kappa^{-2} y_t(\kappa u), \qquad y_t(0) = 1, \tag{B1}$$

$$\tilde{T}_m = \frac{\varepsilon}{3}\kappa^{-2} t = \frac{2T}{\varepsilon}\left( \varepsilon I_1 \Big|_{m=1} m^\theta \right), \tag{B2}$$

where $I_1$ is the one-loop integral from field theory and $\theta = d - 2 + 2\zeta$ is the energy exponent. Note that there is a whole family of solutions as per rescaling invariance. With these definitions, the fixed point equation becomes

$$\partial_u \left[ u y_t(u) - \frac{1}{2}\partial_u (y_t(u) - 1)^2 + t y_t'(u) \right] = 0. \tag{B3}$$

One can then solve this for $y_t$ and relate it to the solution at $t = 0$. Using this, together with rescaling invariance to define

$$\tilde{y}_t(u) = \frac{1}{1+t'} y_{t'}(u\sqrt{1+t'}), \tag{B4}$$

$$t' = \frac{t}{1-t}, \tag{B5}$$

yields

$$\tilde{y}_t(u) = y_0\left( \sqrt{u^2 - \frac{2t}{t+1} + 2\ln(t+1)} \right) \tag{B6}$$

$$\simeq y_0(\sqrt{u^2 + t^2}). \tag{B7}$$

The last equation defines the thermal boundary layer. The parameter $t$ is

$$\frac{t}{\rho} = \frac{3}{\varepsilon}\frac{2Tm^2}{\Delta(0)}. \tag{B8}$$

This works pretty well in the simulation (see Fig. 3).


[1] H. Barkhausen, *Zwei mit Hilfe der neuen Verstärker entdeckte Erscheinungen*, Phys. Ztschr. **20** (1919) 401–403.

[2] G. Durin, F. Bohn, M.A. Correa, R.L. Sommer, P. Le Doussal and K.J. Wiese, *Quantitative scaling of magnetic avalanches*, Phys. Rev. Lett. **117** (2016) 087201, arXiv:1601.01331.

[3] P. Cizeau, S. Zapperi, G. Durin and H. Stanley, *Dynamics of a Ferromagnetic Domain Wall and the Barkhausen Effect*, Phys. Rev. Lett. **79** (1997) 4669–4672.

[4] C. ter Burg, G. Durin and K.J. Wiese, *Universal force-force correlations in Barkhausen experiments*, to be published (2021).

[5] P. Le Doussal, K.J. Wiese, S. Moulinet and E. Rolley, *Height fluctuations of a contact line: A direct measurement of the renormalized disorder correlator*, EPL **87** (2009) 56001, arXiv:0904.4156.

[6] B. Gutenberg and C.F. Richter, *Frequency of earthquakes in California*, Bulletin of the Seismological Society of America **34** (1944) 185.

[7] B. Gutenberg and C.F. Richter, *Earthquake magnitude, intensity, energy, and acceleration*, Bulletin of the Seismological Society of America **46** (1956) 105–145.

[8] Kay Jorg Wiese, Mathilde Bercy, Lena Melkonyan and Thierry Bizebard, *Universal force correlations in an rna-dna unzipping experiment*, Physical Review Research **2** (2020).

[9] P. Le Doussal and K.J. Wiese, *How to measure Functional RG fixed-point functions for dynamics and at depinning*, EPL **77** (2007) 66001, cond-mat/0610525.

[10] A.A. Middleton, P. Le Doussal and K.J. Wiese, *Measuring functional renormalization group fixed-point functions for pinned manifolds*, Phys. Rev. Lett. **98** (2007) 155701, cond-mat/0606160.

[11] A. Rosso, P. Le Doussal and K.J. Wiese, *Numerical calculation of the functional renormalization group fixed-point functions at the depinning transition*, Phys. Rev. B **75** (2007) 220201, cond-mat/0610821.

[12] K.J. Wiese, M. Bercy, L. Melkonyan and T. Bizebard, *Universal force correlations in an RNA-DNA unzipping experiment*, Phys. Rev. Research **2** (2020) 043385, arXiv:1909.01319.

[13] C. ter Burg and K.J. Wiese, *Mean-field theories for depinning and their experimental signatures*, Phys. Rev. E **103** (2021) 052114, arXiv:2010.16372.

[14] L. Balents and P. Le Doussal, *Thermal fluctuations in pinned elastic systems: field theory of rare events and droplets*, Ann. Phys. (NY) **315** (2005) 213–303, cond-mat/0408048.

[15] B. Alessandro, C. Beatrice, G. Bertotti and A. Montorsi, *Domain-wall dynamics and Barkhausen effect in metallic ferromagnetic materials. I. Theory*, J. Appl. Phys. **68** (1990) 2901.

[16] B. Alessandro, C. Beatrice, G. Bertotti and A. Montorsi, *Domain-wall dynamics and Barkhausen effect in metallic ferromagnetic materials. II. Experiments*, J. Appl. Phys. **68** (1990) 2908.

[17] A.A. Middleton, *Asymptotic uniqueness of the sliding state for charge-density waves*, Phys. Rev. Lett. **68** (1992) 670–673.

[18] Y.G. Sinai, *The limiting behaviour of a one-dimensional random walk in a random environments*, Theory Probab. Appl. **27** (1983) 256–268.

[19] Pierre Le Doussal, *Exact results and open questions in first principle functional rg*, Annals of Physics **325** (2010) 49–150.

[20] K.J. Wiese, *Theory and experiments for disordered elastic manifolds, depinning, avalanches, and sandpiles*, (2021), arXiv:2102.01215.

[21] P. Le Doussal and K.J. Wiese, *Driven particle in a random landscape: disorder correlator, avalanche distribution and extreme value statistics of records*, Phys. Rev. E **79** (2009) 051105, arXiv:0808.3217.

[22] J. M. Huguet, N. Forns and F. Ritort, *Statistical properties of metastable intermediates in dna unzipping*, Phys. Rev. Lett. **103** (2009) 248106.